Design Optimization for Improved Tiltrotor Whirl Flutter Stability

Eric Hathaway* Farhan Gandhi†

Rotorcraft Center of Excellence
Department of Aerospace Engineering
The Pennsylvania State University
229 Hammond Building
University Park, PA 16802

Abstract

The results of a formal design optimization study to improve tiltrotor whirl flutter stability are reported. The analysis used in this investigation considers some design parameters which have not been explicitly examined in the literature, such as the distribution of blade flexibility inboard and outboard of the pitch bearing. While previous studies have investigated the individual influence of various design parameters, the present investigation uses formal optimization techniques to determine a unique combination of parameters that maximizes whirl flutter stability. Constraints on the optimization are selected that prevent unrealistically large changes in the design parameters. The influence of rotor and wing design parameters are first considered separately, after which concurrent optimization studies are conducted. Emphasis is placed on a physical interpretation of the optimization results, to better understand the means by which certain combinations of design variables improve stability. The rotor parameters with the greatest influence on flutter speed are pitch-flap and pitch-lag couplings in the rotor blade and the distribution of flap flexibility inboard of the pitch bearing. The important wing parameters are wing vertical bending and torsion stiffness and vertical bending-torsion coupling. Changes in the rotor design parameters provide a greater stabilizing influence than changes in the wing parameters. Optimized designs are presented which require only modest changes in design parameters, while substantially improving whirl flutter stability. For the XV-15 rotor used as a baseline for this study, an optimized configuration obtained while imposing tight constraints on the design parameters increased flutter speed from 310 knots to 450 knots. If the constraints on the design parameters are relaxed, flutter speed may be increased beyond the speed range considered in this investigation.

1 Introduction

Tiltrotor aircraft combine the vertical take-off and landing capability of a helicopter with the speed and range of a conventional fixed-wing aircraft. At high speeds, however, tiltrotors are susceptible to whirl flutter, an aeroelastic instability caused by coupling of rotor-generated aerodynamic forces with elastic wing modes. The conventional approach to ensuring adequate whirl flutter stability margins has required wing structures with very high torsional stiffness, to provide sufficient separation between wing beam bending and torsion frequencies (Ref. 1). This stiffness requirement leads to rather thick wing sections, typically about a 23% thickness-to-chord ratio for current tiltrotor aircraft. The large aerodynamic drag associated with such thick wing sections is an obstacle to achieving the higher cruise speeds envisioned for future tiltrotor aircraft. It is therefore desirable to explore alternative methods for providing the required aeroelastic stability margins.

The mechanism of tiltrotor whirl flutter instability has received considerable experimental and analytical attention [2–10]. Perturbation aerodynamic forces generated on the rotor act on the wing/pylon support structure, exciting wing motions which in turn are fed back to the rotor. As airspeed increases, the magnitude of the destabilizing aerodynamic forces also increases, until an instability is encountered at some critical flutter speed. The complex interaction of rotor and wing degrees of freedom may be influenced by many different design parameters. Numerous studies have investigated the influence of various rotor and wing design parameters on whirl flutter stability.

In Ref. 2, Hall experimentally and analytically investigated the stability characteristics of the Bell XV-3. Reduced rotor pylon mounting stiffness was found to be destabilizing. Increased coupling between blade flapping and the rotor control system (δ_3 coupling) was also destabilizing. In Ref. 3, Young and Lytwyn examined the influence of blade flap stiffness on stability, and found that a fundamental flap frequency of approximately 1.1–1.2/rev provided the greatest stabilizing influence. In Ref. 4, however, Wernicke and

*Graduate Research Assistant, student member AHS
†Associate Professor, member AHS

Proceedings of the 29th European Rotorcraft Forum,
16–18 September 2003, Friedrichshafen, Germany

Gaffey point out that other design considerations such as blade loads and transient flapping response during maneuvers may preclude taking advantage of this ideal frequency placement for enhanced stability. Gaffey, Yen, and Kvaternik (Ref. 7) described the influence of various rotor and wing design parameters on aeroelastic stability, and also discussed the limits imposed on these parameters by other design constraints. Johnson (Ref. 10) developed an analytical model which included elastic blade bending and torsion modes. The primary influence of blade torsion dynamics was reported to be a destabilizing pitch-lag coupling introduced to the rotor by blade flexibility outboard of the pitch bearing. Increased control system stiffness was shown to reduce the destabilizing effect.

More recent studies have continued to examine the influence of many different design parameters, including: rotor and wing stiffness properties [11], various kinematic couplings arising from hub and control system geometry [12], advanced geometry rotor blades (tip sweep, taper, and anhedral) [13], composite couplings in the wing [14, 15] and rotor blades [11, 15], and blade center-of-gravity and aerodynamic-center offsets [16–19]. Introduction of aeroelastic couplings into the wing and rotor have generally been reported to improve whirl flutter stability.

In the references cited above, the various parameters under consideration in each study were *individually* varied. Differences in the analyses and model configurations between the various studies make comparisons of the relative effectiveness of all the design variables difficult. Furthermore, the influence of *optimal combinations* of various design variables has not been explored. Other design considerations besides aeroelastic stability (such as limits on allowable blade loads or rotor transient flapping) may prevent the designer from fully exploiting the stabilizing influence of any one design parameter. Small changes in several design parameters may be able to provide the required gains in stability while still respecting other design constraints.

The focus of the present study is to identify combinations of design parameters which provide the greatest improvement in whirl flutter stability. In addition to the design parameters generally considered in the literature (such as wing/rotor stiffness properties or aeroelastic couplings), the analysis used in this investigation considers some design parameters which have not been examined in previous studies, such as the distribution of blade flexibility inboard and outboard of the pitch bearing. Stability trends of the various design parameters are identified through a parametric study, and formal optimization techniques used to determine a unique combination of parameters that maximizes tiltrotor whirl flutter stability. Constraints on the optimization are selected that prevent unrealistically large changes in the design parameters. The process of formulating a properly posed optimization problem in order to achieve the desired stability characteristics is also discussed. The influence of rotor and wing design parameters are first considered separately, after which concurrent optimization studies are conducted. Emphasis is placed on a physical interpretation of the optimization results, to better understand the means by which certain combinations of design variables improve stability.

2 Analytical Model

The analytical model used in the present investigation was developed in Ref. 20. The model represents a proprotor with three or more blades, mounted on a semi-span, cantilevered wing structure. The point of attachment between the rotor hub and the wing/pylon system can undergo three displacements (x, y, z) and three rotations $(\alpha_x, \alpha_y, \alpha_z)$. The mass, damping, and stiffness properties associated with these degrees of freedom derive from the wing/pylon structure. The rotor hub may be gimballed, allowing cyclic flapping motion at the blade root (β_G). In the fixed frame, this gimbal degree of freedom allows for longitudinal (β_{GC}) and lateral (β_{GS}) tilting of the rotor disk.

The blade is attached to the hub with some pre-cone angle, β_P. Perturbation of rotor azimuthal position in the rotating frame (ψ_s) is included, allowing a windmilling rotor condition to be modeled. Blade flapping motion (β) and in-plane lead-lag motion (ζ) are also included. The model used to represent blade flap and lag flexibility, its distribution with respect to the pitch bearing, and its implications on system behavior, will be described in more detail later.

The rotor aerodynamic model is based on quasi-steady blade element theory. The rotor is assumed to operate in purely axial flow. Prandtl-Glauert compressibility corrections are applied to the aerodynamic model. These corrections are essential for accurate stability predictions, since compressibility directly influences the magnitude of the aerodynamic forces which cause whirl flutter instability. Perturbations in blade pitch are related to gimbal, blade flap, and blade lag motion through aeroelastic coupling parameters.

$$\delta\theta = -K_{P\!G}\beta_G - K_{P\beta}\beta - K_{P\zeta}\zeta \qquad (1)$$

The coupling parameter $K_{P\!G}$ (positive for gimbal flap-up, pitch-down) relates perturbation changes in blade pitch to perturbation gimbal motion β_G. This coupling is typically the result of rotor control system kinematics, and can be specified in terms of a "δ_3" angle through the relation $K_{P\!G} = \tan\delta_3$. The pitch-flap coupling parameter $K_{P\beta}$ (positive for flap-up, pitch-down) and pitch-lag coupling parameter $K_{P\zeta}$ (positive for lag-back, pitch-down) relate changes in blade pitch to blade flap and lag deflections. Potential sources of pitch-flap and pitch-lag coupling include

composite tailoring [11, 15], advanced geometry blade tips [13], or blade CG and AC offsets [16–19]. In the present analysis, terms which describe the pitch-flap and pitch-lag couplings that arise due to blade flexibility outboard of the pitch bearing (described below) are included.

The semi-span cantilevered wing model used in the present analysis is based upon the model developed by Johnson in Ref. 9. The wing is represented using only the first three structural modes: vertical bending (q_1), chordwise bending (q_2), and torsion (p). Offsets of the wing, pylon, and rotor centers of gravity relative to the wing elastic axis are considered which may couple wing bending and torsion motion. In addition to these inertial couplings which are present in Johnson's original model, elastic coupling parameters have been added to the present analysis. These parameters may represent wing bending-torsion coupling due to composite tailoring of the wing structure. The vertical bending-torsion coupling parameter K_{Pq1} and chordwise bending-torsion coupling parameter K_{Pq2} are included in the wing structural stiffness matrix as off-diagonal coupling terms. The wing structural stiffness matrix can then be written as:

$$\begin{bmatrix} K_{q1} & 0 & K_{Pq1} \\ 0 & K_{q2} & K_{Pq2} \\ K_{Pq1} & K_{Pq2} & K_p \end{bmatrix} \tag{2}$$

where K_{q1}, K_{q2}, K_p, are the fundamental stiffnesses associated with the wing modes.

2.1 Blade Structural Flap-Lag Coupling due to Flexibility Distribution

The present analysis models the distribution of blade flexibility inboard and outboard of the pitch bearing which results in a structural flap-lag coupling (SFLC) of the rotor blades. This formulation has been used previously in helicopter rigid-blade stability analyses [21, 22]. Blade flap and lag stiffness is modeled using a set of orthogonal "hub" springs $(K_{\beta H}, K_{\zeta H})$ inboard of the pitch bearing, and orthogonal "blade" springs $(K_{\beta B}, K_{\zeta B})$ outboard of the pitch bearing (see Fig. 1). The relative angle between the hub and blade springs $(\bar{\theta})$ varies as the blade springs rotate with changes in collective pitch. This series of hub and blade springs may be equivalently described in terms of effective flap and lag flexural stiffnesses (K_β, K_ζ) and structural flap-lag coupling parameters (R_β, R_ζ) which define the distribution of flap and lag flexibility inboard and outboard of the pitch bearing.

$$K_\beta = \frac{K_{\beta H} K_{\beta B}}{K_{\beta H} + K_{\beta B}} \quad \text{and} \quad K_\zeta = \frac{K_{\zeta H} K_{\zeta B}}{K_{\zeta H} + K_{\zeta B}} \tag{3}$$

$$R_\beta = \frac{K_\beta}{K_{\beta B}} \quad \text{and} \quad R_\zeta = \frac{K_\zeta}{K_{\zeta B}} \tag{4}$$

In Eq. (4), a value of $R_\beta = 0$ describes a blade where all the flap flexibility is located inboard of the pitch bearing, and $R_\beta = 1$ represents a blade where all the flap flexibility is outboard of the pitch bearing. The distribution of lag flexibility varies similarly, but with parameter R_ζ. See Ref. 22 for a detailed description of this formulation.

Note that the terms "flap" and "lag" in the above description may be somewhat misleading. At the high collective pitch settings required to trim the rotor in cruise, the blade "flap" and "lag" springs are rotated such that the primary source of stiffness for in-plane blade motion is actually K_β (assuming a rotor where most of the flexibility is located outboard of the pitch bearing). The "flap stiffness" in the SFLC formulation physically corresponds most closely to the blade flatwise bending stiffness, and "lag stiffness" corresponds to chordwise bending stiffness. For clarity, blade stiffness properties will henceforth be discussed in terms of flatwise and chordwise bending stiffnesses.

Using the definitions of blade stiffness given above, the elastic flap and lag restoring moments may be written as

$$\begin{Bmatrix} M_\beta \\ M_\zeta \end{Bmatrix} = [K_{\text{eff}}] \begin{Bmatrix} \beta \\ \zeta \end{Bmatrix} = \begin{bmatrix} K_{\beta\beta} & K_{\beta\zeta} \\ K_{\beta\zeta} & K_{\zeta\zeta} \end{bmatrix} \begin{Bmatrix} \beta \\ \zeta \end{Bmatrix} \tag{5}$$

where K_{eff} represents an effective stiffness matrix, the individual terms of which are defined as

$$\begin{aligned} K_{\beta\beta} &= \frac{1}{\Delta}\left[K_\beta + \left(R_\beta K_\zeta - R_\zeta K_\beta\right)\sin^2\bar{\theta}\right] \\ K_{\zeta\zeta} &= \frac{1}{\Delta}\left[K_\zeta - \left(R_\beta K_\zeta - R_\zeta K_\beta\right)\sin^2\bar{\theta}\right] \\ K_{\beta\zeta} &= -\frac{1}{\Delta}\left(R_\beta K_\zeta - R_\zeta K_\beta\right)\cos\bar{\theta}\sin\bar{\theta} \end{aligned} \tag{6}$$

and

$$\begin{aligned} \Delta = 1 &+ \left(2R_\beta R_\zeta - R_\beta - R_\zeta\right)\sin^2\bar{\theta} \\ &+ \left[R_\zeta\left(1-R_\zeta\right)\frac{K_\beta}{K_\zeta} + R_\beta\left(1-R_\beta\right)\frac{K_\zeta}{K_\beta}\right]\sin^2\bar{\theta} \end{aligned} \tag{7}$$

Tiltrotor aircraft may experience large changes in blade flap and lag mode frequencies due to the large changes in collective pitch required to trim the rotor over the entire flight speed range. Equations (5)–(7) show that in the present model, the effective blade flap and lag stiffness is a function of collective pitch $\bar{\theta}$. By selecting proper values of the fundamental blade flatwise and chordwise stiffnesses K_β and K_ζ, and coupling parameters R_β and R_ζ, the variation of blade flap and lag frequency with collective pitch may be modeled directly. This is unlike many rigid blade tiltrotor stability analyses, which require blade flap and lag frequency variations be provided explicitly as inputs to the analysis.

2.2 Pitch-Flap and Pitch-Lag Couplings due to Blade Flexibility Distribution

The present analysis includes expressions for pitch-flap and pitch-lag coupling parameters which capture the influence of blade flexibility distribution (inboard/outboard of the pitch bearing) on aeroelastic stability. These couplings act to reduce the whirl flutter stability boundary. Figures 2 and 3 show the predicted modal frequency and damping variation versus airspeed for the baseline XV-15 full-scale semi-span model. Figure 4 shows the damping characteristics when the pitch-flap and pitch-lag coupling terms are neglected. Comparing the stability boundary in Fig. 4 to the stability boundary in Fig. 3 shows that these couplings are responsible for a substantial decrease in the predicted flutter speed. The derivation of terms representing the contribution of blade flap and lag flexibility distribution to the overall pitch-flap and pitch-lag couplings is summarized below, to show how various rotor design variables can influence the magnitude of these couplings. Reference 20 contains a more detailed examination of the origins of pitch-flap and pitch-lag couplings due to the distribution of blade flexibility.

Considering the distribution of flap and lag flexibility inboard and outboard of the pitch bearing described in the SFLC formulation above, the total flap and lag displacement of the blade may be defined (assuming small rotations) as the sum of flap and lag displacements inboard and outboard of the pitch bearing.

$$\begin{Bmatrix} \beta \\ \zeta \end{Bmatrix} = \begin{Bmatrix} \beta_{\text{in}} \\ \zeta_{\text{in}} \end{Bmatrix} + \begin{Bmatrix} \beta_{\text{out}} \\ \zeta_{\text{out}} \end{Bmatrix} \tag{8}$$

When the blade undergoes flap and lag motions, the feather axis of the blade undergoes a rotation of β_{in} out-of-plane and ζ_{in} in-plane. At the same time, the blade itself undergoes rotations of β_{out} and ζ_{out} relative to the feather axis, as shown in Fig. 5. These motions must be considered when formulating the blade pitch equations of motion.

The flap and lag motions inboard of the pitch bearing $(\beta_{\text{in}}, \zeta_{\text{in}})$ and the motions outboard of the pitch bearing $(\beta_{\text{out}}, \zeta_{\text{out}})$ can be expressed as fractions of the total flap and lag angles (β, ζ). In Ref. 20, expressions relating the deflections inboard and outboard of the pitch bearing to the total flap and lag angles were defined as:

$$\begin{Bmatrix} \beta_{\text{in}} \\ \zeta_{\text{in}} \end{Bmatrix} = \begin{bmatrix} A & B \\ C & D \end{bmatrix} \begin{Bmatrix} \beta \\ \zeta \end{Bmatrix} \tag{9}$$

$$\begin{Bmatrix} \beta_{\text{out}} \\ \zeta_{\text{out}} \end{Bmatrix} = \begin{bmatrix} W & X \\ Y & Z \end{bmatrix} \begin{Bmatrix} \beta \\ \zeta \end{Bmatrix} \tag{10}$$

where

$$\begin{aligned} A &= \frac{1}{\Delta}\left[1 - R_\beta + \left(R_\zeta - \frac{K_\zeta}{K_\beta}R_\beta\right)(R_\beta - 1)\sin^2\bar{\theta}\right] \\ B &= -\frac{1}{\Delta}\left(R_\zeta - \frac{K_\zeta}{K_\beta}R_\beta\right)(R_\beta - 1)\sin\bar{\theta}\cos\bar{\theta} \\ C &= \frac{1}{\Delta}\left(R_\beta - \frac{K_\beta}{K_\zeta}R_\zeta\right)(R_\zeta - 1)\sin\bar{\theta}\cos\bar{\theta} \\ D &= \frac{1}{\Delta}\left[1 - R_\zeta + \left(R_\beta - \frac{K_\beta}{K_\zeta}R_\zeta\right)(R_\zeta - 1)\sin^2\bar{\theta}\right] \end{aligned} \tag{11}$$

and

$$\begin{aligned} W &= \frac{1}{\Delta}\left[R_\beta + \left(R_\beta - \frac{K_\beta}{K_\zeta}R_\zeta\right)(R_\zeta - 1)\sin^2\bar{\theta}\right] \\ X &= -B \\ Y &= -C \\ Z &= \frac{1}{\Delta}\left[R_\zeta + \left(R_\zeta - \frac{K_\zeta}{K_\beta}R_\beta\right)(R_\beta - 1)\sin^2\bar{\theta}\right] \end{aligned} \tag{12}$$

(The term Δ in Eqs. (11) and (12) is given in Eq. (7).)

Equations (9)–(12) show that the relative amount of flap and lag motion inboard and outboard of the pitch bearing is determined by the fundamental blade flap and lag stiffnesses K_β and K_ζ, the SFLC parameters R_β and R_ζ, and by the collective pitch setting.

Now consider the forces and moments on the blade which contribute to the blade pitch equation of motion. Figure 6 illustrates the forces acting on a representative section of the blade outboard of the pitch bearing. The figure is oriented such that the blade's feather axis is directly out of the page. In addition to the terms which are part of the fundamental pitch dynamics, there are in-plane (F_x) and out-of-plane (F_z) forces acting on the blade section which have moment arms about the feather axis due to blade flap and lag displacements outboard of the pitch bearing $(\beta_{\text{out}}, \zeta_{\text{out}})$. This creates a coupling between blade pitching motion and blade flap and lag motions. Reference 20 showed that effective pitch-flap and pitch-lag coupling parameters could be extracted from the blade pitch equations of motion. These coupling terms, derived from

first principles, capture the influence of the distribution of blade flexibility inboard and outboard of the pitch bearing on aeroelastic stability. The couplings are given as (from Ref. 20)

$$\widetilde{K}_{P\beta} = \frac{1}{K_\theta}\begin{bmatrix} 2(YK_{\beta\beta} - WK_{\beta\zeta})\bar{\beta}_0 \\ +(ZK_{\beta\beta} - (X-Y)K_{\beta\zeta} - WK_{\zeta\zeta})\bar{\zeta}_0 \end{bmatrix} \quad (13)$$

$$\widetilde{K}_{P\zeta} = \frac{1}{K_\theta}\begin{bmatrix} (ZK_{\beta\beta} - (X-Y)K_{\beta\zeta} - WK_{\zeta\zeta})\bar{\beta}_0 \\ +2(ZK_{\beta\zeta} - XK_{\zeta\zeta})\bar{\zeta}_0 \end{bmatrix} \quad (14)$$

where $\bar{\beta}_0$ and $\bar{\zeta}_0$ are the trim flap and lag angles, and K_θ is the stiffness of the blade pitch control system. Figure 7 shows the variation of the pitch-flap and flap-lag coupling parameters with airspeed for the XV-15 semi-span model. The magnitude of the couplings given by Eqs. (13) and (14) is influenced by several factors. The distribution of blade flap and lag flexibility determines how much blade flap and lag motion occurs outboard of the pitch bearing. Smaller values of the SFLC parameters R_β and R_ζ will yield less flap and lag motion outboard of the pitch bearing, reducing the magnitude of the pitch-flap and pitch-lag couplings. If all the blade flexibility is inboard of the pitch bearing ($R_\beta, R_\zeta = 0$), the pitch-flap and pitch-lag couplings in Eqs. (13) and (14) are eliminated. Similarly, a stiffer control system (increased K_θ) will reduce the couplings by constraining blade pitch motion. For the case of infinite control system stiffness, the couplings are eliminated.

In the present analysis, the *total* pitch-flap and pitch-lag coupling can be represented as

$$K_{P\beta}^{\text{total}} = \widetilde{K}_{P\beta} + \Delta K_{P\beta} \quad (15)$$

$$K_{P\zeta}^{\text{total}} = \widetilde{K}_{P\zeta} + \Delta K_{P\zeta} \quad (16)$$

where the terms $\Delta K_{P\beta}$ and $\Delta K_{P\zeta}$ are additional design variables introduced to represent the influence of other potential sources of pitch-flap and pitch-lag coupling in the rotor blades, such as composite tailoring, blade CG and AC offsets, or advanced blade tip shapes such as sweep and anhedral. The influence of these design parameters on whirl flutter stability stems largely from the coupling between blade bending and pitch that these parameters introduce. While the present analysis does not attempt to model these sources of pitch-flap and pitch-lag coupling in detail, the parameters $\Delta K_{P\beta}$ and $\Delta K_{P\zeta}$ may serve as a general representation of the couplings arising from any or all of these sources.

2.3 Validation

Figures 8 and 9 provide sample validation results obtained using the present analysis. Figure 8 plots wing beam mode damping versus velocity for the full-scale semi-span XV-15 model tested at NASA Ames in the early 1970s (Ref. 9). The figure compares predictions from the present analysis with results from two elastic blade analyses (Refs. 10 and 11) as well as experimental data from Ref. 9. The figure shows good agreement between all three models and the experimental data.

A full-scale rotor designed for the Boeing Model 222 tiltrotor was also tested at NASA Ames, in 1972. Unlike the stiff-inplane, gimballed XV-15 rotor, the Model 222 rotor was a soft-inplane, hingeless design. Figure 9 shows wing vertical bending mode damping versus airspeed. The present analysis agrees closely with the results from Johnson's elastic blade formulation from Ref. 10, and both analyses correlate well with the available experimental data from Ref. 9.

Additional validation results may be found in Ref. 20.

3 Parametric Study

Before beginning formal optimization studies, a parametric study is conducted. The study provides an understanding of the influence of individual design variables on whirl flutter stability. The tiltrotor configuration used is the full-scale XV-15 semi-span model. Table 1 lists some of the important model parameters used in the present analysis (see Ref. 9 for a more complete listing of model properties).

3.1 Influence of Individual Rotor Design Parameters

The rotor design parameters considered in this investigation are: *(1)* blade flatwise bending stiffness, in terms of the non-rotating natural frequency $\omega_{\beta 0}$, *(2)* blade chordwise bending stiffness, in terms of the non-rotating natural frequency $\omega_{\zeta 0}$, *(3)* gimbal spring stiffness, denoted by $\omega_{\beta G0}$, the non-rotating gimbal frequency, *(4)* pitch-gimbal coupling, expressed as a "δ_3" angle, *(5)* blade pitch-flap coupling parameter, $\Delta K_{P\beta}$, which is added to $\widetilde{K}_{P\beta}$ (Eq. (13)) to obtain the total pitch-flap coupling, *(6)* blade pitch-lag coupling parameter $\Delta K_{P\zeta}$, which is added to $\widetilde{K}_{P\zeta}$ (Eq. (14)) to obtain the total pitch-lag coupling, *(7)* distribution of blade flatwise bending flexibility, R_β, and *(8)* chordwise bending flexibility, R_ζ (inboard/outboard of the pitch bearing), and *(9)* control system stiffness, expressed in terms of the frequency ω_ϕ. The nominal value for each of these design variables for the baseline configuration are given in Table 1.

Changes in some of the rotor design parameters considered in this study influence the magnitudes of $\widetilde{K}_{P\beta}$ and $\widetilde{K}_{P\zeta}$, the pitch-flap and pitch-lag couplings due to blade flexibility distribution given by Eqs. (13) and (14). These couplings have a powerful influence on whirl flutter stability (compare Figs. 3 and 4), and it is useful to identify whether the primary impact on whirl flutter from a change in a given parameter is due to a direct influence on the system dynamics (such as through a change in modal characteristics), or from its effect on the magnitude of pitch-flap and pitch-lag coupling. For the parameters which influence the magnitude of these couplings, results will also be examined for a case where the distributions of $\widetilde{K}_{P\beta}$ and $\widetilde{K}_{P\zeta}$ remain fixed to their baseline values (shown in Fig. 7). Thus the influence of each design variable on overall whirl flutter stability can be better understood.

Figures 10–19 show the influence of the various rotor design variables on the critical whirl flutter speed. The influence of the various design variables may be summarized as follows:

1. Altering the blade flatwise and chordwise bending stiffness properties can influence stability two ways. The change in blade stiffness will affect the variation of rotor frequencies with collective pitch, influencing the interaction between rotor and wing modes. In addition, a change in blade stiffness affects the magnitude of the destabilizing pitch-flap and pitch-lag couplings given in Eqs. (13) and (14). In the case of increased flatwise bending stiffness (Fig. 10), the stabilizing influence comes mainly through the change in rotor frequencies. Increased flatwise bending stiffness increases the frequency of the rotor lag modes. The shift in low-frequency cyclic lag mode frequency in particular changes the interaction of that mode with the wing modes, increasing damping in the wing modes. Increased flatwise bending stiffness slightly reduces the magnitude of $\widetilde{K}_{P\zeta}$, but also slightly increases the magnitude of $\widetilde{K}_{P\beta}$, so the net influence of the changes in pitch-flap and pitch-lag coupling is negligible. If the influence of changes in blade flatwise bending stiffness on flutter speed was examined while holding $\widetilde{K}_{P\beta}$ and $\widetilde{K}_{P\zeta}$ to their baseline values, the results would be almost exactly the same as shown in Fig. 10.

   For reduced chordwise bending stiffness (Fig. 11), the increased stability comes almost entirely through a decrease in the magnitude of $\widetilde{K}_{P\zeta}$. Negative pitch-lag coupling as calculated by Eq. (14) is reduced by a third at high speeds, from about -0.3 to -0.2, while the pitch-flap coupling from Eq. (13) remains virtually unchanged. Figure 12 illustrates the reduction in $\widetilde{K}_{P\zeta}$ as a result of reduced chordwise bending stiffness. If $\widetilde{K}_{P\beta}$ and $\widetilde{K}_{P\zeta}$ are held to the baseline values shown in Fig. 7, changes in blade chordwise bending stiffness have almost no influence on flutter speed.

2. Increased gimbal spring stiffness has only a slight beneficial influence on flutter speed. In Ref. 11, changes in cyclic flap frequency (equivalent to gimbal natural frequency in the present analysis) had a somewhat larger effect on stability than in the present analysis. However, the range of frequency variation considered in Ref. 11 (0.9–2.5/rev) is much larger than in the present analysis and is unlikely to be attainable in practice. Reference 4 points out that although increased flapping restraint can be stabilizing, design constraints on allowable blade loads place an upper limit on flap restraint stiffness which may preclude taking advantage of this parameter to increase aeroelastic stability. In the present analysis, a variation in $\Delta\omega_{\beta G0}$ of $\pm 100\%$ corresponds to a rotating frequency variation of 1–1.07/rev. Since the XV-15's gimbal spring is composed of a relatively soft elastomeric material, changes in stiffness required to achieve a $\pm 100\%$ change in $\Delta\omega_{\beta G0}$ are feasible.

3. The δ_3 angle (Fig. 13) gives rise to a coupling between blade pitch and gimbal flapping, and has a strong influence on aeroelastic stability. The baseline value of δ_3 for the XV-15 is -15^o. In Fig. 13, we can see that more negative values of δ_3 are very destabilizing. The maximum increase in flutter speed occurs as δ_3 approaches 0^o, followed by a sharp decrease in flutter speed for positive δ_3 angles, as a rotor mode instability is encountered. These results are consistent with the descriptions in Ref. 6 and elsewhere of the influence of δ_3 on stiff-inplane proprotor stability.

   The baseline δ_3 angle of -15^o represents a trade-off between conflicting design requirements, as described in Ref. 7. Larger (more negative) values of δ_3 are desirable to minimize transient blade flapping response, while a δ_3 angle close to zero is beneficial for aeroelastic stability. Furthermore, due to geometric constraints, it is difficult to design a control mechanism with a δ_3 angle close to zero, especially for gimballed rotors which have effectively zero flapping hinge-offset. For these reasons, it may be difficult to exploit reduced δ_3 angles to improve tiltrotor aeroelastic stability, and it may in fact be desirable to identify design configurations which allow for larger negative values of δ_3 while still maintaining adequate stability boundaries.

4. The design variables $\Delta K_{P\beta}$ in Fig. 14 and $\Delta K_{P\zeta}$ in Fig. 15 refer to an additional value of pitch-flap and pitch-lag coupling, respectively, that are

added to the couplings due to blade flexibility distribution to obtain the total values of blade pitch-flap and pitch-lag coupling. Positive values of additional pitch-flap (Fig. 14) and pitch-lag (Fig. 15) couplings are both stabilizing. Positive pitch-lag coupling has a particularly strong stabilizing influence. This is consistent with the findings reported in Refs. 11 and 15, where composite couplings that produced lag-back, pitch-down motions in the blade were stabilizing.

It should be noted in Fig. 15 that the stabilizing influence of $\Delta K_{P\zeta}$ becomes particularly strong as the parameter reaches values near +0.3. At high airspeeds near the flutter boundary, the baseline level of pitch-lag coupling due to blade flexibility distribution calculated in Eq. (14) is approximately -0.3 (see Fig. 7). The critical flutter speed in Fig. 15 increases most sharply when the positive pitch-lag coupling from $\Delta K_{P\zeta}$ completely offsets the negative contribution from $\widetilde{K}_{P\zeta}$. Thus, the important criteria to ensure a beneficial influence on aeroelastic stability is that the *total* level of pitch-lag coupling (amount of coupling from Eq. (14) plus any pitch-lag coupling contribution from other sources) in the rotor be positive (lag-back, pitch-down).

5. The influence of blade flexibility distribution inboard and outboard of the pitch bearing is examined in Figs. 16 and 18. As was the case for blade stiffness, changes in blade flexibility distribution may influence stability by directly changing the variation of blade frequencies with collective pitch, or by effecting the magnitude of $\widetilde{K}_{P\beta}$ and $\widetilde{K}_{P\zeta}$, the pitch-flap and pitch-lag couplings due to blade flexibility distribution. Figure 16 shows that R_β, the distribution of blade flatwise bending flexibility, is a powerful parameter. As the flap flexibility inboard of the pitch bearing increases (the parameter R_β becomes smaller), the amount of pitch-flap and pitch-lag coupling from Eqs. (13) and (14) is reduced sharply (as shown in Fig. 17), increasing the flutter speed. It is this observation that provides the motivation for the use of a flexured hub on the V-22. The hub's coning flexure allows more trim elastic coning deflection to take place inboard of the blade pitch bearing, thus minimizing the undesirable coupling, as reported in Ref. 23. Moving some of the blade flatwise bending flexibility inboard of the pitch bearing also influences the variation of rotor lag frequency with collective pitch. Figure 16 shows that even if $\widetilde{K}_{P\beta}$ and $\widetilde{K}_{P\zeta}$ are held to their baseline values, increased flap flexibility inboard of the pitch bearing still has some stabilizing influence. As was the case for increased blade flatwise bending stiffness, this stability increase is due to a change in the nature of the interaction of the rotor low-frequency cyclic lag mode with the wing modes. The total influence of changes in the parameter R_β on whirl flutter stability is thus a result of both rotor frequency changes and a reduction in the destabilizing pitch-flap and pitch-lag couplings.

   Increased blade chordwise flexibility inboard of the pitch bearing (Fig. 18) has a slightly destabilizing influence on stability. Reducing the parameter R_ζ from its baseline value of 1 causes a stabilizing positive increase in $\widetilde{K}_{P\zeta}$, but also a destabilizing negative change in $\widetilde{K}_{P\beta}$. The net influence of these changes in pitch-flap and pitch-lag couplings on stability is negligible. The primary source of the slightly destabilizing effect of increased chordwise flexibility inboard of the pitch bearing is through a change in the variation of rotor frequencies with collective pitch. Holding $\widetilde{K}_{P\beta}$ and $\widetilde{K}_{P\zeta}$ to their baseline values has little effect on the influence of R_ζ on stability.

6. The influence of control system stiffness (Fig. 19) on whirl flutter stability is due to its effect on the magnitude of $\widetilde{K}_{P\beta}$ and $\widetilde{K}_{P\zeta}$ (Eqs. (13) and (14)). As the control system stiffness increases, flutter speed also increases, since a stiffer control system reduces the destabilizing couplings due to blade flexibility distribution. This is consistent with observations in Refs. 10 and 23. If $\widetilde{K}_{P\beta}$ and $\widetilde{K}_{P\zeta}$ are held fixed to their baseline values, changes in control system stiffness have no influence on the predicted stability boundary.

3.2 Influence of Individual Wing Design Parameters

The wing design parameters considered in the present study are *(1)* wing vertical bending stiffness (K_{q1}), *(2)* chordwise bending stiffness (K_{q2}), *(3)* torsional stiffness (K_p), *(4)* vertical bending-torsion coupling (K_{Pq1}), and *(5)* chordwise bending-torsion coupling (K_{q2}). The bending-torsion coupling represented by the parameters K_{Pq1} and K_{Pq2} may come from several sources, including composite tailoring of the wing structure, wing sweep, or mass offsets of the wing or rotor/nacelle structure, relative to the wing elastic axis. The findings of a parametric study of the influence of these wing stiffness and coupling parameters on whirl flutter stability may be summarized as follows:

1. Reduced vertical bending stiffness increases the stability of the wing vertical bending mode, while slightly destabilizing the chordwise bending and torsion modes. Figure 20 shows how changes in the wing vertical bending stiffness influence flutter speed. This observation is consistent with the

results reported in Refs. 7, 11, and 24. While decreased wing stiffness is generally destabilizing for whirl flutter, decreased vertical bending stiffness increases the frequency separation between the vertical bending mode and torsion mode, reducing the amount of coupling between wing vertical bending and torsion motion. This interpretation of the influence of reduced vertical bending stiffness is confirmed by examination of the eigenvectors produced by the stability analysis. For typical tiltrotor configurations, wing vertical bending and torsion motions are inertially coupled through the mass of the rotor and nacelle which is offset from the wing elastic axis. When the separation between wing vertical bending and torsion mode frequencies is increased, there is less pitching motion of the nacelle in the wing vertical bending mode, which reduces the amount of blade flapping and thus reduces the destabilizing rotor aerodynamic forces acting on the wing. Figure 20 shows that if the natural frequency of the vertical bending mode is reduced by about 17%, the mode is completely stabilized.

2. Figure 21 shows that reduced wing torsional stiffness is destabilizing, particularly in the case of the vertical bending mode. This is again due to the fact that reduced torsional stiffness reduces the frequency separation between the vertical bending mode and torsion mode and increases the coupling between wing vertical bending and torsion motion. Figure 21 illustrates the need for very thick, torsionally stiff wings in current tiltrotor designs. Even a modest reduction in wing torsion stiffness would result in an unacceptable decrease in flutter speed. Increased torsional stiffness, on the other hand, is not a desirable design solution, since increasing the torsional stiffness would require even thicker wing sections, increasing aerodynamic drag.

3. The analysis shows very little sensitivity to changes in wing chordwise bending stiffness. This is consistent with Ref. 7, where changes in wing chordwise stiffness within the typical design range had little influence on flutter speed.

4. Figure 22 illustrates the influence of wing vertical bending-torsion coupling. Positive values of the coupling parameter K_{Pq1} (which in the present analysis denotes a wing bend up/twist nose down coupling) have a beneficial influence on the critical vertical bending mode, and are only slightly destabilizing for the other modes, yielding an overall increase in flutter speed. This additional elastic coupling introduced in the wing opposes the inherent inertial coupling due to the offset mass of the rotor and nacelle at the wing tip. Thus the overall coupling of wing vertical bending and torsion motion is reduced, as was the case for reduced vertical bending stiffness. The beneficial influence of vertical bending-torsion coupling in the wing has been reported in Refs. 1, 14, 15.

5. Wing chordwise bending-torsion coupling (Fig. 23) has virtually no influence on flutter speed boundaries for the baseline wing/rotor configuration. Negative values of the coupling parameter K_{Pq2} do slightly improve the subcritical damping of the wing chordwise bending mode, however. References 1 and 14 do not note any stability benefits from wing chordwise bending-torsion coupling. In Ref. 15 however, chordwise bending-torsion coupling was reported to be strongly stabilizing for tiltrotor whirl flutter. The source of the discrepancy between these studies and the reported influence of chordwise bending-torsion coupling in Ref. 15 is unclear. It is possible that differences in the tiltrotor configuration used to perform the study are responsible for the discrepancy. The wing chordwise bending and torsion motions were reported to be coupled in Ref. 15, while the configuration used in the present analysis shows little coupling of these motions.

4 Parametric Optimization

After developing an understanding of the influence of the individual design parameters on whirl-flutter stability, formal optimization techniques are used to identify combinations of these design variables that improve the vehicle's whirl-flutter stability characteristics.

4.1 Formulation

A gradient-based algorithm is used to perform the parametric optimization. This routine attempts to minimize a user-defined objective function $F(D_j)$, where D_j is the vector of design parameters considered in the optimization. The optimizer calculates sensitivity gradients, $\partial F/\partial D_j$, numerically by individually perturbing each design variable. Based on these gradients, a steepest-descent search direction is determined, and a new combination of design variables is selected. This procedure is repeated until the objective function reaches a minimum value (i.e. when $\partial F/\partial D_j = 0$), or the design variables have all reached their user-specified limits. For the purposes of this optimization study, three sets of constraints on the design parameters are considered: relaxed, moderate, and tight constraints. In an actual tiltrotor design, constraints based on considerations such as weight, allowable loads, and transient rotor flapping would prevent the designer from making arbitrarily large changes in the

design parameters in order to improve aeroelastic stability. A small change in any one design parameter may not provide sufficient stability gains. The tight set of constraints is formulated to examine what increases in stability may be obtained through relatively modest changes to many design variables simultaneously. The moderate and relaxed sets of constraints further show what additional gains in stability are possible if larger changes to the design parameters are permitted by the overall design constraints. The three sets of constraints on the design parameters are given in Table 2. Nominal values for each design parameter (corresponding to the XV-15 full-scale semi-span model) are provided in Table 1.

Since the optimization uses a gradient-based approach, the optimizer may return a locally optimal solution, instead of the global optimum. To avoid this problem, the optimization was repeatedly performed, with random initial starting points. Different "optimized" solutions were returned for some initial conditions, indicating that local minima do exist in the design space. Performing the optimization repeatedly allowed locally optimal solutions to be discarded in favor of globally optimized configurations.

4.2 Selection of Objective Function

In order to obtain a satisfactory design solution from the optimization, the objective function $F(D_j)$ must be well-posed. Selection of a proper objective function can often be a trial-and-error process, where several candidate functions are tested before a function is identified which most effectively achieves the intended goal of the optimization. The goal of the optimization in general is to increase the whirl flutter stability boundary. Additionally, it is desirable to avoid "cliff-type" instabilities, where the transition from a stable to an unstable condition occurs rapidly over a very small speed range.

Initial efforts to improve whirl flutter stability by formulating an objective function that sought to improve damping of the wing vertical bending mode (the critical flutter mode of the baseline configuration) were unsuccessful. Combinations of design parameters which increased damping in the selected mode were often strongly destabilizing for some other mode. To achieve satisfactory design solutions, the optimization must be formulated to improve the damping of the *least-damped* mode, whichever mode that may be. Thus, for each iteration of the optimization, the critical mode must be re-identified, since changes to the design parameters in the course of the optimization may cause different modes to become critical. Furthermore, attempts to improve whirl flutter stability by formulating an objective function to increase damping at some given velocity produced unacceptable design configurations. Performing the optimization at only one airspeed tended to produce designs that displayed sharp decreases in stability just beyond the optimization speed. In addition, in some cases the damping of several modes at low speed was degraded from the baseline configuration. While most of this reduction in damping occurred at or below the speed where a tiltrotor would begin the transition to helicopter mode, it is not generally desirable to achieve increased damping at high speeds at the expense of reduced damping at lower speeds.

To address these issues, and produce significant stability margins over a range of flight speeds, a *moving point* optimization is conceived. The objective function is written as

$$\text{maximize } F(D_j) = \zeta_{\min}|_{V=200\rightarrow 600\,\text{kts}} \qquad (17)$$

Over a range of speeds from 200 to 600 knots, the optimizer attempts to maximize the damping at the point of least damping within that range. As the design variables are adjusted in each iteration of the optimization, this point may shift to a different airspeed. Thus for each iteration of the optimization, the airspeed corresponding to the point of minimum damping must first be identified. The search for the airspeed at which damping is lowest can be formulated as a minimization problem (Find the airspeed V such that $\zeta_{\min}$ is at a minimum), and placed within the main optimization loop. The same gradient-based optimization routine used to determine optimal combinations of the design variables can then also be used to locate the airspeed at which the optimization is to occur. This two-stage optimization process may be summarized by the following flowchart:

Main Optimization Loop

1) Inner−Loop Optimization

minimize $F(V) = \zeta_{\min}\big|_{D_j}$

Iterate until Converged

(identifies $V_{\min}$, the velocity at which damping is at a minimum)

2) maximize $F(D_j) = \zeta_{\min}\big|_{V_{\min}}$

$D_j = [\,\Delta\omega_{\beta 0} \quad \Delta\omega_{\zeta 0} \quad \ldots\,]$

Iterate until Converged

(identifies new set of design variables D_j which maximizes damping at $V_{\min}$)

For each iteration, using the current set of rotor design variables, the optimizer first determines the airspeed V at which the damping is lowest. An iteration of the optimization is then performed at that airspeed V obtained from the inner loop optimization. Sensitiv-

ity gradients for each of the design variables are calculated at the current design point and the design variables are updated, yielding a new configuration which is tested for optimality. If the design is not yet optimal, the optimization procedure is repeated, first re-identifying the airspeed where damping is minimum for the new configuration. Such an optimization algorithm was originally conceived in Ref. 25 to optimize rotor design variables to alleviate helicopter ground resonance. See Ref. 25 for further discussion of the algorithm.

The upper and lower limits of the speed range over which the optimizer seeks to improve damping were selected after experimenting with several different values. The lower bound of 200 knots was set low enough to ensure that the optimized configuration would not trade off damping at low speed for gains in stability at higher speeds closer to the flutter boundary, but not so low that the optimizer is trying to increase the damping of modes that are inherently lightly damped at very low speeds. The upper limit of 600 knots was set well above the maximum speed of conventional tiltrotor aircraft. This ensures that any sharp "cliff-type" instabilities will only occur well above the tiltrotor's maximum speed.

4.3 Optimization of Rotor Parameters

A moving point optimization attempting to maximize damping over the range of 200-600 kts was performed, using each of the three previously defined sets of bounds on the design parameters. Table 3 provides the resulting values of the optimized design parameters.

The damping characteristics of the configuration optimized with tight constraints are shown in Fig. 24. Note that for this optimization, each design parameter has reached either its upper or lower limit. Comparing the optimized design to the parametric study results shows that each parameter follows the stabilizing trend identified in the parametric study. Even though only small changes to the baseline configuration are allowed by the tight bounds on the design parameters, the optimized configuration was still able to substantially improve the flutter speed by about 130 knots, from 310 to 440 knots.

The influence of each design parameter on the final configuration is examined by individually setting each parameter in turn to it's baseline value and examining the resulting stability prediction. Using this procedure, it was determined that the majority of the increase in damping over the baseline is produced by the change in the parameters $\Delta K_{P\beta}$, $\Delta K_{P\zeta}$, and R_β. Leaving these parameters set to the optimal values given in the first column of Table 3 and returning the others to their baseline values yielded a configuration with a flutter speed of 409 knots, still almost a 100 knot increase over the baseline.

Figure 25 shows the damping characteristics of the configuration optimized with the intermediate set of constraints. As was the case when optimizing with the tight bounds, each design parameter has reached either its upper or lower limit. The values of each parameter are again consistent with the stability trends identified in the parametric study. The greater freedom allowed by the intermediate bounds allows for an optimized configuration that stabilizes the system up to 600 knots, with damping levels of at least 2.7% critical over that range. Examining the contribution of each design parameter to the overall stability reveals that, in addition to $\Delta K_{P\beta}$, $\Delta K_{P\zeta}$, and R_β, the δ_3 angle also provides an important contribution. For the tight set of bounds, the upper limit on δ_3 was set to it's baseline value of -15^o. The intermediate constraints allowed δ_3 to increase to 0^o, providing a stabilizing influence on the wing modes, as shown in the parametric study. Retaining only the optimized values of $\Delta K_{P\beta}$, $\Delta K_{P\zeta}$, R_β, and δ_3 yielded a configuration which still remained stable to 600 knots, with at least 2% damping from 200 to 600 knots.

Figure 26 shows that the configuration obtained using the relaxed bounds is stable to 600 knots, with at least 4.3% critical damping from 200 to 600 knots. While many of the design parameters in the optimized configuration have reached an upper or lower bound, some have not. The δ_3 angle has remained near the value obtained when optimizing with the intermediate bounds. The parametric study results showed that positive values of δ_3 quickly brought on a rotor mode instability (see Fig. 13), and that maximum flutter speed was obtained for values of δ_3 near zero. Similarly, for the distribution of blade flatwise bending stiffness inboard and outboard of the pitch bearing, the parametric study showed that flutter speed was maximized for values of R_β near 0.5, while further reductions in R_β had little effect on flutter speed. For the configuration optimized with relaxed bounds, changes in the other design variables have shifted this maximum slightly, resulting in an optimal value of R_β of 0.344. This shift in blade flexibility has a large influence on the pitch-flap and pitch-lag couplings given by Eqs. (13) and (14). Reduced R_β greatly reduces the negative pitch-lag coupling due to pitch dynamics, as shown in Fig. 27, which compares the variation of $\widetilde{K}_{P\beta}$ and $\widetilde{K}_{P\zeta}$ with airspeed for the baseline configuration and the configuration optimized with the relaxed constraints. Figure 27 shows that $\widetilde{K}_{P\zeta}$ is actually positive for the optimized configuration. Since $\widetilde{K}_{P\zeta}$ is already positive, there is little need for the parameter $\Delta K_{P\zeta}$ to provide further positive coupling. This is why the optimized configuration only requires a moderate positive value for $\Delta K_{P\zeta}$.

As with the configuration optimized with intermediate bounds, the biggest improvement in stability is due

to the influence of the parameters $\Delta K_{P\beta}$, $\Delta K_{P\zeta}$, R_β, and δ_3. Since the optimal values of δ_3 may not be feasible due to blade transient flapping considerations, the key rotor design changes required for improving whirl flutter stability are additional positive blade pitch-flap and pitch-lag coupling (positive $\Delta K_{P\beta}$ and $\Delta K_{P\zeta}$) and increased blade flatwise bending flexibility inboard of the pitch bearing ($R_\beta < 1$). It should be noted that more recent tiltrotor designs than the XV-15 rotor used in this study may already have a value of R_β less than one due to the presence of a coning flexure, as used in the V-22 rotor hub. The primary influence of all three of these design parameters is to cause a net positive change in the *total* pitch-flap and pitch-lag couplings (Eqs. (15) and (16)) by reducing (in the case of R_β) or offsetting (by positive $\Delta K_{P\beta}$ and $\Delta K_{P\zeta}$) the negative pitch-flap and pitch-lag couplings due to the distribution of blade flexibility. The results of this rotor parameter optimization study indicate that whirl flutter stability can be maximized by achieving positive total pitch-flap and pitch-lag couplings.

4.4 Optimization of Wing Parameters

The optimization process is repeated, this time considering only the wing stiffness and coupling parameters as design variables. Initial attempts at improving stability through optimization using the objective function in Eq. (17) did not produce satisfactory results. The problem is illustrated in Fig. 28, which shows the damping of the wing modes for the baseline configuration. The figure shows that the vertical bending mode is the critical mode, becoming unstable at 310 knots. At speeds above 400 knots, however, all three wing modes are unstable and both the chordwise bending and torsion modes are more unstable than the vertical bending mode. An optimization process seeking to satisfy the objective function of Eq. (17) will first seek a configuration that increases damping at the point of lowest damping in the speed range under consideration. For the baseline configuration shown in Fig. 28, the optimization would seek to increase the damping of the torsion mode at high speed. Unfortunately, as shown in the wing parametric study results (Figs. 20–23), changes in the wing design parameters do not significantly improve wing chord or torsion mode stability, so the optimization is unable to proceed. The optimization never even gets around to attempting to improve damping of the critical vertical bending mode.

To obtain favorable configurations of wing design parameters, the objective function must be restricted to operate only in regions where the design parameters are effective at increasing the damping of the critical mode. This is achieved by reducing the upper bound on the range of airspeeds considered in the optimization from 600 knots to 300 knots. Therefore, the objective function used to optimize the wing design parameters is now:

$$\text{maximize } F(D_j) = \zeta_{\min}|_{V=200\rightarrow 300\,\text{kts}} \qquad (18)$$

Optimized combinations of the wing design parameters obtained by using the objective function in Eq. (18) and the three different sets of constraints (Table 2) are shown in Table 4.

Figure 29 shows the damping characteristics of the configuration obtained using the tight constraints on the design variables. Table 4 shows that each design parameter has reached a limit imposed on it by the tight constraints, and the optimized values are in agreement with the stability trends identified in the parametric study. Using this optimized configuration, the stability boundary of the critical vertical bending mode is increased from 310 to 340 knots. This increase in flutter speed is due almost entirely to the influence of the design parameters $\Delta\omega_{q1}$, $\Delta\omega_p$, and K_{Pq1}. As was observed in the parametric study, increased frequency separation between the wing vertical bending and torsion modes (such as is provided by decreased ω_{q1} and increased ω_p) and positive vertical bending-torsion coupling improve the stability of the vertical bending mode. The other two design parameters, $\Delta\omega_{q2}$ and K_{Pq2}, have a much smaller influence on the overall damping, providing only a very slight increase in damping.

The stability characteristics of the configuration optimized with the intermediate set of constraints are shown in Fig. 30. Comparing the performance of this design to that of the tightly-constrained optimized configuration (Fig. 29) reveals that the vertical bending mode is further stabilized, actually becoming stable over the entire speed range considered in this study. There is however only a marginal gain in actual flutter speed relative to the design using tight constraints, since the chordwise bending mode is now the critical mode, and the wing design parameters are unable to significantly improve the damping of that mode.

Examining the values (given in Table 4) of the design parameters obtained using the intermediate set of constraints shows that all of the variables follow the same trends seen in the parametric study and reach either an upper or lower bound, except for the chordwise bending-torsion coupling parameter, K_{Pq2}. This is due to the fact that positive K_{Pq2} slightly increases vertical bending mode damping, while slightly reducing chordwise bending mode damping. For the optimized configuration obtained using tight variables, over the speed range considered by the optimization (200 to 300 knots), the vertical bending mode damping is always lower than the chordwise bending mode damping. For the configuration using intermediate constraints, near 300 knots the damping of the vertical and chordwise bending modes are nearly equal. Thus if the value of K_{Pq2} is either increased or decreased, the

damping of one of the two modes would be decreased. It should be noted however that the additional damping provided by K_{Pq2} is very small.

Optimization of Eq. (18) using the relaxed constraints yields a configuration with damping characteristics shown in Fig. 31. As was the case for the configuration optimized using the intermediate constraints, relaxing the constraints allows for further gains in vertical bending mode damping, but flutter speed is unchanged, since the chord mode stability boundary is not strongly influenced by any of the wing design parameters. As shown in Table 4, the parameters $\Delta\omega_{q1}$, $\Delta\omega_{q2}$, and K_{Pq1} continue to follow the trends shown in the parametric study. Compared to the previous wing optimization results, the change in torsion frequency, $\Delta\omega_p$, and the chordwise bending-torsion coupling parameter K_{Pq2} have now changed sign. This is again due to the fact that these parameters have conflicting influences on damping of the vertical and chordwise bending modes. The optimization process balances these effects on damping of the two modes, increasing the damping of both of them as much as possible. Figure 31 shows that over most of the speed range considered by the optimization, the level of damping in the vertical and chordwise bending modes is the same.

The results presented in this study of wing design optimization show that there is an upper limit on the stability gains that can be achieved by changes in the wing design parameters. Modest changes in the wing vertical bending and torsion mode stiffnesses ($\Delta\omega_{q1}$ and $\Delta\omega_p$) and wing vertical bending-torsion coupling (K_{Pq1}) improve the stability of the critical wing vertical bending mode. However, none of the wing design parameters are able to significantly influence stability of the wing chordwise bending and torsion modes. Once the vertical bending mode is sufficiently stabilized such that chordwise bending becomes the critical mode, larger changes in wing design parameters are ineffective in further increasing the critical whirl flutter speed.

4.5 Concurrent Wing/Rotor Optimization

An optimization is performed which considers both rotor and wing design parameters simultaneously. Because of the much greater influence of the rotor parameters on damping, the concurrent wing/rotor optimization study is restricted to the tight set of constraints. Equation (17) is used as the objective function. Table 5 lists the design configuration resulting from this optimization. Figure 32 shows the damping characteristics of the design. The optimized configuration has a stability boundary of 435 knots, a 125 knot increase over the baseline. For comparison, optimizing rotor parameters alone using the tight constraints produced a flutter speed of 440 knots, and using the wing parameters alone yielded a 340 knot flutter speed.

The fact that the concurrent optimization produces a design with a lower flutter speed than optimization of the rotor parameters alone indicates there is a problem with the concurrent optimization as it is originally posed. As was the case for the wing parameter optimization, performing the concurrent optimization from 200 to 600 knots causes the optimizer to select values for the wing design parameters that are (slightly) beneficial to the wing chord and torsion modes at high speed, but do not provide as great a benefit to the critical vertical bending mode as is possible. However, it is not desirable to use the objective function used for the wing optimization study (Eq. (18)) for the concurrent optimization, because reducing the upper limit of the speed range under consideration will prevent the optimization from taking full advantage of the rotor design parameters.

To perform a useful concurrent optimization, a new objective function is formulated. Instead of attempting to increase damping at a certain speed or over a range of speeds, the objective function is formulated to maximize the flutter speed of the system, the speed at which the first instability is encountered. The objective function is thus written as:

$$\text{maximize } F(D_j) = V_{\text{flutter}} \tag{19}$$

where V_{flutter} is the airspeed at which the damping of any system mode goes to zero. It should be noted that the objective function in Eq. (19) would not be suitable for an optimization performed using the intermediate or relaxed constraints on rotor parameters, since the rotor parameters would then be powerful enough to drive the critical flutter speed beyond the upper limit on airspeed considered in the study. Once the upper limit on airspeed was reached, the optimization would make no effort to improve stability by increasing the subcritical damping, as is the case when optimizing using Eq. (17).

The results of a concurrent wing/rotor parameter optimization using Eq. (19) as the objective function are also provided in Table 5. Figure 33 shows the stability characteristics of this configuration. The optimization to maximize flutter speed produced a design with a flutter speed of 450 knots, a 140 knot increase over the baseline configuration. The values of the optimized rotor design parameters are the same as the values obtained when optimizing rotor parameters alone. The wing parameters $\Delta\omega_{q1}$ and K_{Pq2} differ from the values they take when wing parameters are optimized alone. This again has to do with a difference in which mode is critical between the wing-only optimization and the concurrent optimization. It is interesting to note that the concurrently optimized design (Fig. 33) only slightly outperforms the design obtained by optimizing only the rotor parameters (Fig. 24). This demonstrates how much more potential is available for improving stability through the rotor variables

than through the wing parameters. Optimizations performed with more relaxed constraints on the wing parameters did not produce configurations that significantly improved on the stability of the configurations given in Table 5.

Throughout this optimization study, it has been pointed out that the design parameters which have the greatest influence on improving whirl flutter stability are: the blade pitch-flap and pitch-lag coupling parameters ($\Delta K_{P\beta}$ and $\Delta K_{P\zeta}$), the distribution of blade flatwise bending stiffness (R_β), change in wing vertical bending and torsion stiffness ($\Delta\omega_{q1}$ and $\Delta\omega_p$), and wing vertical bending-torsion coupling (K_{Pq1}). A tightly constrained optimization using the objective function in Eq. (19) was performed using only these key parameters as design variables. Table 5 provides the resulting optimized values of these design parameters. Figure 34 shows that the damping characteristics using only the key parameters is quite similar to the case shown in Fig. 33, where all design parameters were considered. The flutter speed attained through modest changes in only the key parameters is 425 knots, still 115 knots above the baseline stability boundary.

5 Concluding Remarks

An analytical investigation of the influence of various rotor and wing design parameters on tiltrotor whirl flutter stability was conducted. The parameters were all examined using the same analysis and same baseline tiltrotor configuration, to allow for comparison of the relative effectiveness of each parameter. In addition to investigating the influence of each parameter individually (as in previous studies), numerical optimization techniques were utilized to identify combinations of the design parameters which could significantly improve tiltrotor whirl flutter stability. Relatively tight constraints on the design parameters were applied, in recognition of the fact that design considerations other than aeroelastic stability preclude large changes in many of the parameters.

The findings of this study may be summarized as follows:

1. The rotor design parameters which have the greatest influence on flutter speed are the additional pitch-flap and pitch-lag coupling parameters ($\Delta K_{P\beta}$ and $\Delta K_{P\zeta}$) and the distribution of blade flap flexibility inboard of the pitch bearing (R_β). These parameters act to increase stability primarily by either offsetting (positive $\Delta K_{P\beta}$ and $\Delta K_{P\zeta}$) or reducing ($R_\beta < 1$) the magnitude of the destabilizing couplings which arise due to blade flexibility outboard of the pitch bearing ($\widetilde{K}_{P\beta}$ and $\widetilde{K}_{P\beta}$). Stability may be maximized by ensuring that the *total* pitch-flap and pitch-lag couplings are positive.

2. The wing design parameters which have the greatest influence on flutter speed are the wing vertical bending and torsion stiffness, and vertical bending-torsion coupling. Reduced vertical bending stiffness, increased torsional stiffness, and positive vertical bending-torsion coupling (bend-up, twist nose-down) all act to reduce the amount of nacelle pitching motion present in the wing vertical bending mode, which is the critical mode for the present model.

3. Flutter speed shows a much stronger sensitivity to changes in the rotor parameters than the wing parameters. Optimization of wing parameters using the relaxed set of constraints produces a design that increases flutter speed by about 50 knots, while optimizing the rotor parameters using the tight constraints on the design variable yields a 130 knot increase in flutter speed.

4. A concurrent optimization of the key rotor and wing design variables provides only a modest increase in flutter speed over configurations resulting from optimization of rotor variables alone.

5. The optimization process produces generally intuitive results. The configurations obtained through formal optimization are consistent with the stability trends identified by individually varying each design parameter.

6. The optimization procedures described in this study can successfully identify combinations of design parameters that increase whirl flutter stability. The optimal designs require only modest changes in the key rotor and wing design parameters in order to significantly increase flutter speed. Such changes may be possible while still respecting other design constraints.

References

[1] Nixon, M. W., Piatak, D. J., Corso, L. M., and Popelka, D. A., "Aeroelastic Tailoring for Stability Augmentation and Performance Enhancement of Tiltrotor Aircraft," Proceedings of the 55th Annual AHS Forum, Montreal, Canada, May 25–27, 1999.

[2] Hall, Jr., W. E., "Prop-Rotor Stability at High Advance Ratios," *Journal of the American Helicopter Society*, vol. 11, no. 2, April 1966, pp. 11–26.

[3] Young, M. I. and Lytwyn, R. T., "The Influence of Blade Flapping Restraint on the Dynamic Stability of Low Disk Loading Propeller-

Rotors," *Journal of the American Helicopter Society*, vol. 12, no. 4, October 1967, pp. 38–54.

[4] Wernicke, K. G. and Gaffey, T. M., "Review and Disscussion of 'The Influence of Blade Flapping Restraint on the Dynamic Stability of Low Disk Loading Propeller-Rotors'," *Journal of the American Helicopter Society*, vol. 12, no. 4, October 1967, pp. 55–60.

[5] Edenborough, H. K., "Investigation of Tilt-Rotor VTOL Aircraft Rotor-Pylon Stability," *Journal of Aircraft*, vol. 5, no. 6, March-April 1968, pp. 97–105.

[6] Gaffey, T. M., "The Effect of Positive Pitch-flap Coupling (Negative δ_3) on Rotor Blade Motion Stability and Flapping," *Journal of the American Helicopter Society*, vol. 14, no. 2, April 1969, pp. 49–67.

[7] Gaffey, T. M., Yen, J. G., and Kvaternik, R. G., "Analysis and Model Tests of the Proprotor Dynamics of a Tilt-Proprotor VTOL Aircraft," Presented at the Air Force V/STOL Technology and Planning Conference, Las Vegas, Nevada, September 23–25, 1969.

[8] Kvaternik, R. G., *Studies in Tilt-Rotor VTOL Aircraft Aeroelasticity*, Ph.D. thesis, Case Western Reserve University, 1973.

[9] Johnson, W., "Dynamics of Tilting Proprotor Aircraft in Cruise Flight," NASA TN D-7677, May, 1974.

[10] Johnson, W., "Analytical Modeling Requirements for Tilting Proprotor Aircraft Dynamics," NASA TN D-8013, July, 1975.

[11] Nixon, M. W., *Aeroelastic Response and Stability of Tiltrotors with Elastically-Coupled Composite Rotor Blades*, Ph.D. thesis, University of Maryland, 1993.

[12] Moore, M. J., Yablonski, M. J., Mathew, B., and Liu, J., "High Speed Tiltrotors: Dynamics Methodology," Proceedings of the 49th Annual AHS Forum, St. Louis, MO, May 19–21, 1993.

[13] Srinivas, V., Chopra, I., and Nixon, M., "Aeroelastic Analysis of Advanced Geometry Tiltrotor Aircraft," *Journal of the American Helicopter Society*, vol. 43, no. 3, July 1998, pp. 212–221.

[14] Popelka, D. A., Lindsay, D., Parham, Jr., T., Berry, V., and Baker, D. J., "Results of an Aeroelastic Tailoring Study for a Composite Tiltrotor Wing," *Journal of the American Helicopter Society*, vol. 42, no. 2, April 1997, pp. 126–136.

[15] Barkai, S. M. and Rand, O., "The Influence of Composite Induced Couplings on Tiltrotor Whirl Flutter Stability," *Journal of the American Helicopter Society*, vol. 43, no. 2, April 1998, pp. 133–145.

[16] Acree, Jr., C. W., Peyran, R. J., and Johnson, W., "Rotor Design for Whirl Flutter: An Examination of Options for Improving Tiltrotor Aeroelastic Stability Margins," Proceedings of the 55th Annual AHS Forum, Montreal, Canada, May 25–27, 1999.

[17] Acree, Jr., C. W., Peyran, R. J., and Johnson, W., "Improving Tiltrotor Whirl-Mode Stability with Rotor Design Variables," Proceedings of the 26th European Rotorcraft Forum, The Hague, The Netherlands, September 2000.

[18] Acree, Jr., C. W., "Effects of Rotor Design Variations on Tiltrotor Whirl-Mode Stability," Tiltrotor/Runway Independent Aircraft Specialists' Meeting of the American Helicopter Society, Arlington, TX, March 20–21, 2001.

[19] Acree, Jr., C. W., "Rotor Design Options for Improving V-22 Whirl-Mode Stability," Proceedings of the 58th Annual AHS Forum, Montreal, Canada, June 11–13, 2002.

[20] Hathaway, E. L. and Gandhi, F., "Modeling Refinements in Simple Tiltrotor Whirl Flutter Analyses," *Journal of the American Helicopter Society*, vol. 48, no. 3, July 2003, pp. 186–198.

[21] Ormiston, R. A. and Hodges, D. H., "Linear Flap-Lag Dynamics of Hingeless Helicopter Rotor Blades in Hover," *Journal of the American Helicopter Society*, vol. 17, no. 2, April 1972, pp. 2–14.

[22] Gandhi, F. and Hathaway, E., "Optimized Aeroelastic Couplings for Alleviation of Helicopter Ground Resonance," *Journal of Aircraft*, vol. 35, no. 4, July–August 1998, pp. 582–590.

[23] Piatak, D. J., Kvaternik, R. G., Nixon, M. W., Langston, C. W., Singleton, J. D., Bennett, R. L., and Brown, R. K., "A Wind-Tunnel Parametric Investigation of Tiltrotor Whirl-Flutter Stability Boundaries," Proceedings of the 57th Annual AHS Forum, Washington, DC, May 9–11, 2001.

[24] Wang, J. M., Jones, C. T., and Nixon, M. W., "A Variable Diameter Short Haul Civil Tiltrotor," Proceedings of the 55th Annual AHS Forum, Montreal, Canada, May 25–27, 1999.

[25] Hathaway, E. and Gandhi, F., "Concurrently Optimized Aeroelastic Couplings and Rotor Stiffness for Alleviation of Helicopter Aeromechanical Instability," *Journal of Aircraft*, vol. 38, no. 1, January–February 2001, pp. 69–80.

Table 1: XV-15 Full-scale Test: Model Properties

Number of blades, N	3
Radius, R	12.5 ft
Lock number, γ	3.83
Solidity, σ	0.089
Lift curve slope, $c_{l\alpha}$	5.7
Rotational speed, Ω	458 RPM
Blade Inertia Properties	
I_b	105 slug-ft^2
I_β	81.8 slug-ft^2
$I_{\beta\alpha}$	105 slug-ft^2
I_ζ	70.4 slug-ft^2
$I_{\zeta\alpha}$	82.6 slug-ft^2
S_β	10.2 slug-ft
S_ζ	8.69 slug-ft
Design Parameters—Nominal Values	
$\omega_{\beta 0}$	59.8 rad/sec
$\omega_{\zeta 0}$	103 rad/sec
$\omega_{\beta G0}$	9.04 rad/sec
δ_3	-15^o
$\Delta K_{P\beta}$	0
$\Delta K_{P\zeta}$	0
R_β	1
R_ζ	1
ω_ϕ	225 rad/sec
ω_{q1}	19.9 rad/sec
ω_{q2}	32.2 rad/sec
ω_p	67.4 rad/sec
K_{Pq1}	0
K_{Pq2}	0

Table 2: Constraints on Design Parameters

	Tight Constraints	Intermediate Constraints	Relaxed Constraints
	(Lower Bound/Upper Bound)		
$\Delta\omega_{\beta 0}$	-5%/+5%	-10%/+10%	-20%/+20%
$\Delta\omega_{\zeta 0}$	-5%/+5%	-10%/+10%	-20%/+20%
$\Delta\omega_{\beta G0}$	-25%/+25%	-50%/+50%	-100%/+100%
δ_3	-15^o/-45^o	0^o/-45^o	+15^o/-45^o
$\Delta K_{P\beta}$	-0.1/0.1	-0.3/0.3	-0.6/0.6
$\Delta K_{P\zeta}$	-0.1/0.1	-0.3/0.3	-0.6/0.6
R_β	0.8/1	0.5/1	0/1
R_ζ	0.8/1	0.5/1	0/1
$\Delta\omega_\phi$	-5%/+5%	-10%/+10%	-20%/+20%
$\Delta\omega_{q1}$	-5%/+5%	-10%/+10%	-20%/+20%
$\Delta\omega_{q2}$	-5%/+5%	-10%/+10%	-20%/+20%
$\Delta\omega_p$	-5%/+5%	-10%/+10%	-20%/+20%
K_{Pq1}	-0.1/0.1	-0.3/0.3	-0.6/0.6
K_{Pq2}	-0.1/0.1	-0.3/0.3	-0.6/0.6

Table 3: Rotor Parameter Optimization Results

	Tight Constraints	Intermediate Constraints	Relaxed Constraints
$\Delta\omega_{\beta 0}$	+5%	+10%	+20.0%
$\Delta\omega_{\zeta 0}$	-5%	-10%	-20%
$\Delta\omega_{\beta G0}$	+25%	+50%	+100%
δ_3	-15^o	0^o	-2.21^o
$\Delta K_{P\beta}$	0.1	0.3	0.6
$\Delta K_{P\zeta}$	0.1	0.3	0.190
R_β	0.8	0.5	0.344
R_ζ	1	1	1
$\Delta\omega_\phi$	+5%	+10%	+20%

Table 4: Wing Parameter Optimization Results

	Tight Constraints	Intermediate Constraints	Relaxed Constraints
$\Delta\omega_{q1}$	-5%	-10%	-20%
$\Delta\omega_{q2}$	+5%	+10%	+20%
$\Delta\omega_p$	+5%	+10%	-11.2%
K_{Pq1}	0.1	0.3	0.572
K_{Pq2}	0.1	0.0714	-0.6

Table 5: Concurrent Wing/Rotor Parameter Optimization Results

	Maximize Damping	Maximize Flutter Speed		
	All Design Parameters		Only Key Parameters	
$\Delta\omega_{\beta 0}$	+5%	+5%	0%	*(fixed)*
$\Delta\omega_{\zeta 0}$	-5%	-5%	0%	*(fixed)*
$\Delta\omega_{\beta G0}$	+25%	+25%	0%	*(fixed)*
δ_3	-15^o	-15^o	-15^o	*(fixed)*
$\Delta K_{P\beta}$	0.1	0.1	0.1	
$\Delta K_{P\zeta}$	0.1	0.1	0.1	
R_β	0.8	0.8	0.8	
R_ζ	1	1	1	*(fixed)*
$\Delta\omega_\phi$	+5%	+5%	0%	*(fixed)*
$\Delta\omega_{q1}$	+5%	+2.07%	+0.104%	
$\Delta\omega_{q2}$	+5%	+5%	0%	*(fixed)*
$\Delta\omega_p$	+5%	+5%	+5%	
K_{Pq1}	-0.1	0.1	0.1	
K_{Pq2}	-0.1	-0.1	0	*(fixed)*

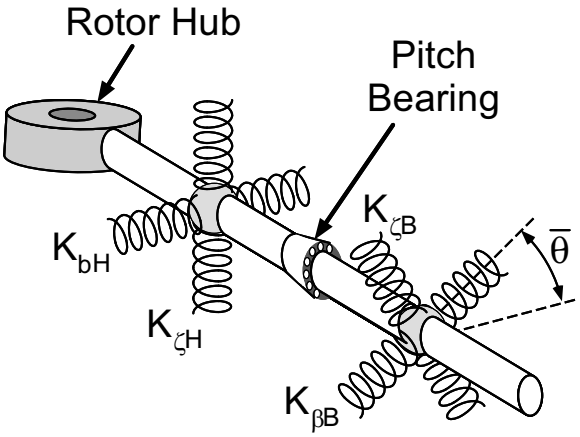

Figure 1: Arrangement of springs used to model blade flap/lag flexibility distribution inboard and outboard of the pitch bearing

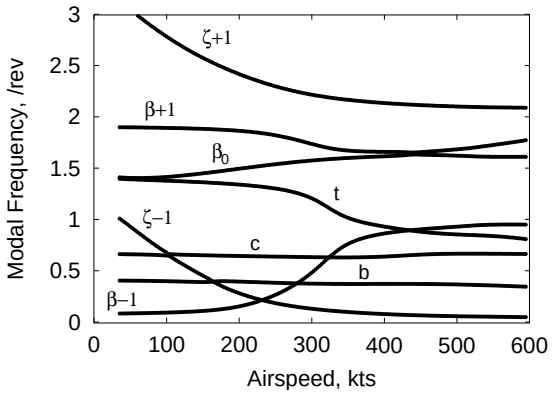

Figure 2: Modal frequencies of baseline system (b: wing beam mode, c: wing chord mode, t: wing torsion mode, β_0: rotor coning mode, $\zeta-1, \zeta+1$: cyclic lag modes, $\beta-1, \beta+1$: cyclic flap (gimbal) modes)

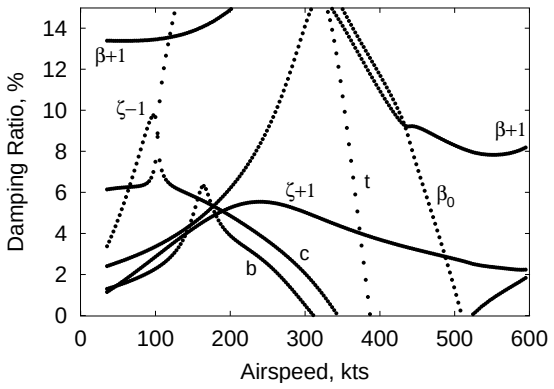

Figure 3: Modal damping of baseline system

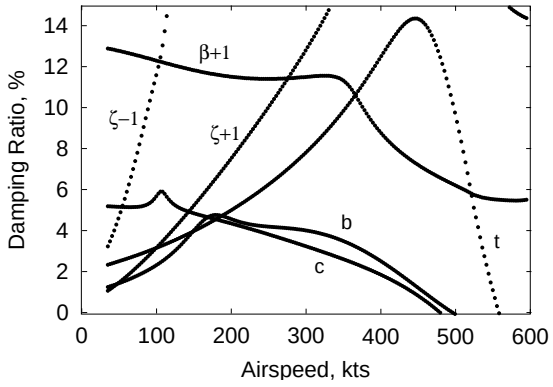

Figure 4: Modal Damping of Baseline System, no couplings due to pitch dynamics

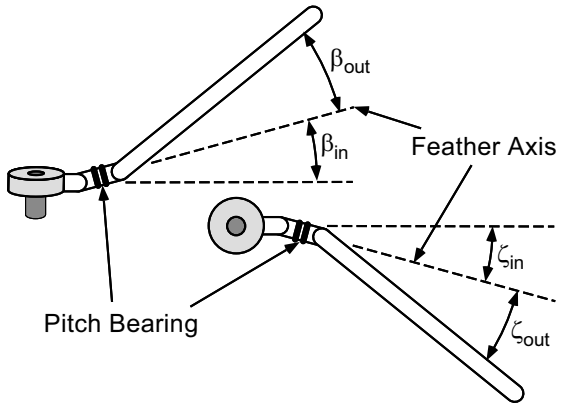

Figure 5: Blade flap and lag angles inboard and outboard of pitch bearing

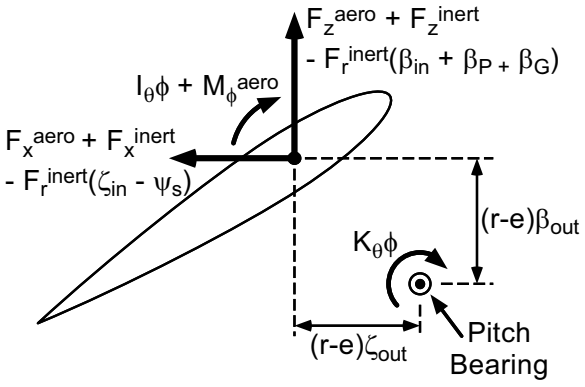

Figure 6: Origin of pitch-flap and pitch-lag couplings—in-plane and out-of-plane forces contribute to blade pitch dynamics due to blade bending outboard of pitch bearing

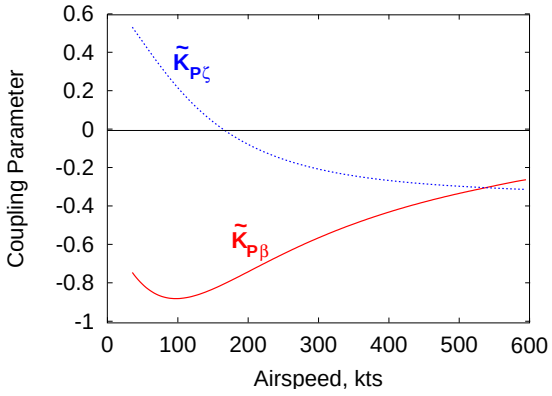

Figure 7: Variation of pitch-flap and pitch-lag coupling parameters (due to flexibility outboard of the pitch bearing) for baseline system

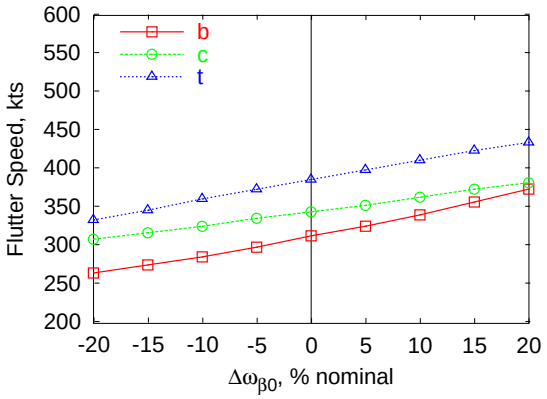

Figure 10: Influence of blade flatwise bending stiffness on flutter speed

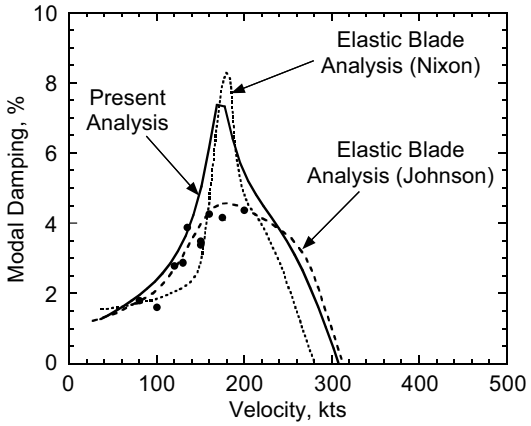

Figure 8: Semi-span XV-15—Damping of wing vertical bending mode vs. airspeed (from Ref. 20)

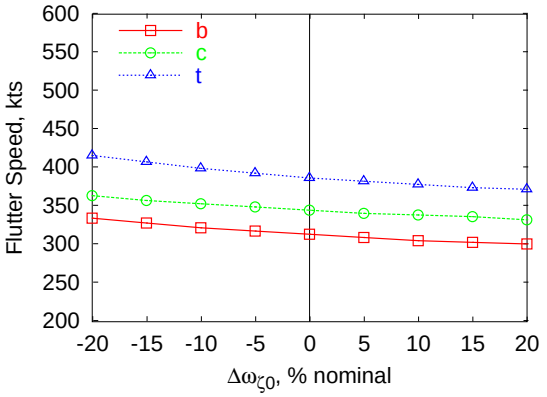

Figure 11: Influence of blade chordwise bending stiffness on flutter speed

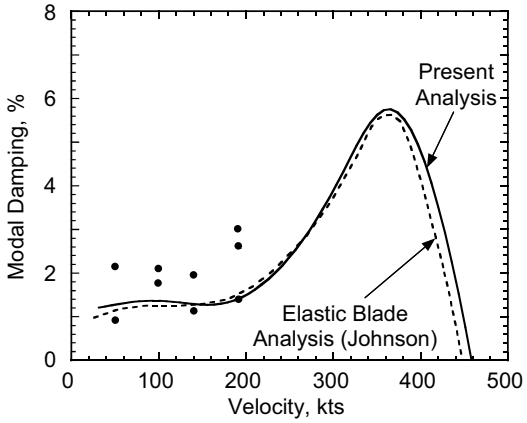

Figure 9: Boeing Model 222—Damping of wing vertical bending mode vs. airspeed (from Ref. 20)

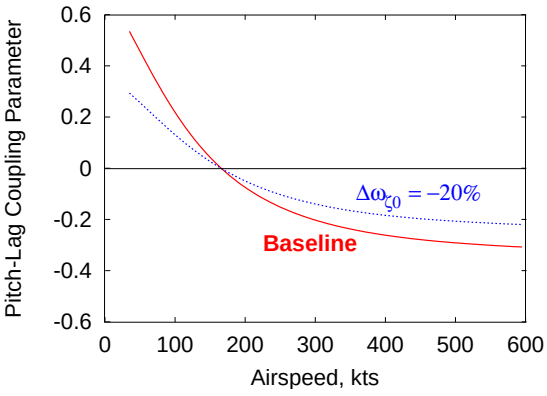

Figure 12: Effect of reduced chordwise bending stiffness on pitch-lag coupling due to blade flexibility distribution $\tilde{K}_{P\zeta}$ (Eq. (14))

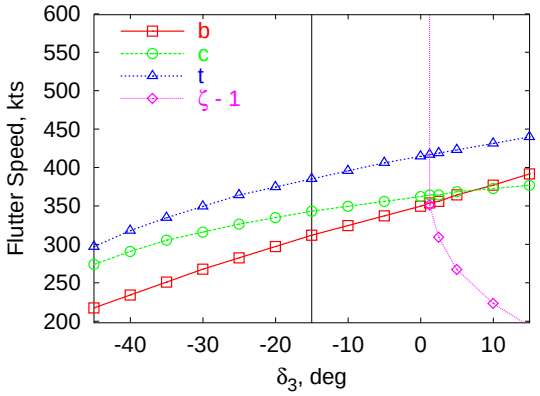

Figure 13: Influence of δ_3 angle (pitch-gimbal coupling) on flutter speed (Baseline $\delta_3 = 15^o$)

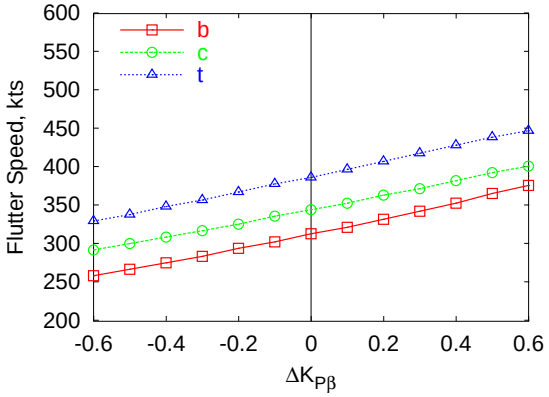

Figure 14: Influence of additional pitch-flap coupling on flutter speed

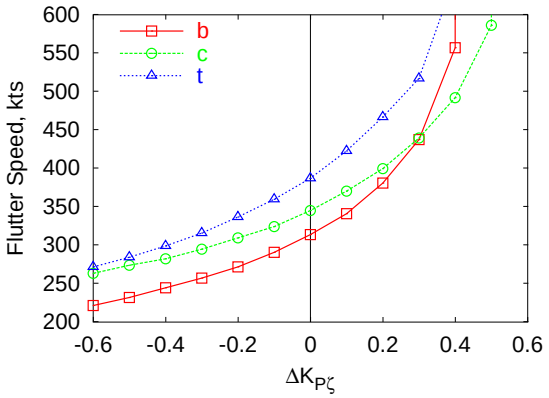

Figure 15: Influence of additional pitch-lag coupling on flutter speed

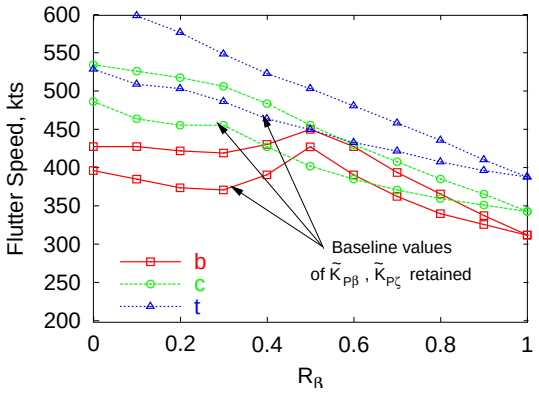

Figure 16: Influence of distribution of blade flatwise bending flexibility on flutter speed (Baseline $R_\beta = 1$)

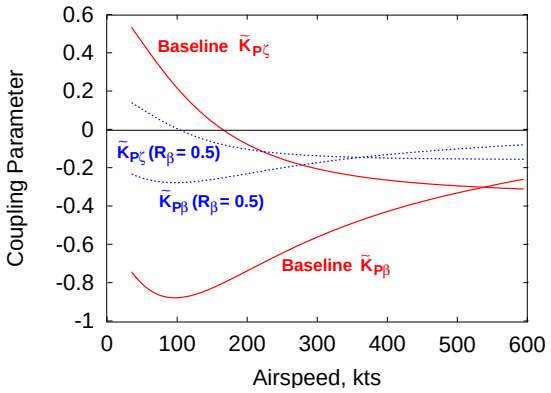

Figure 17: Influence of reduced R_β on couplings due to blade flexibility distribution (Baseline $R_\beta = 1$)

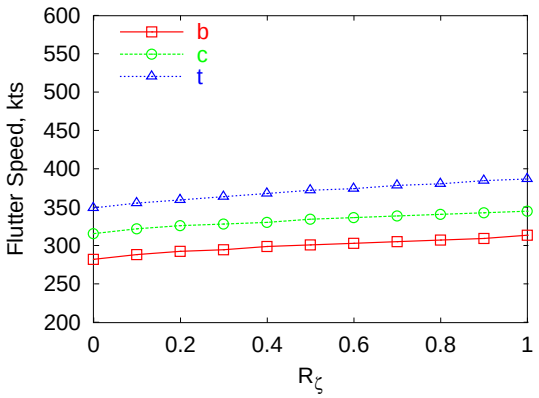

Figure 18: Influence of distribution of blade chordwise bending flexibility on flutter speed (Baseline $R_\zeta = 1$)

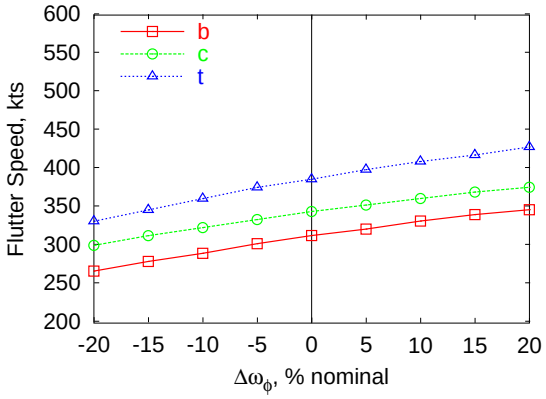

Figure 19: Influence of control system stiffness on flutter speed

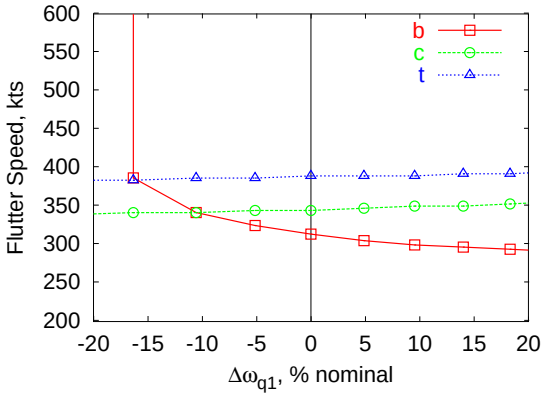

Figure 20: Influence of wing vertical bending stiffness on flutter speed

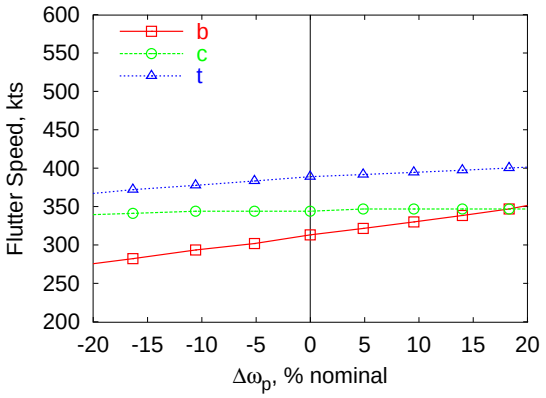

Figure 21: Influence of wing torsional stiffness on flutter speed

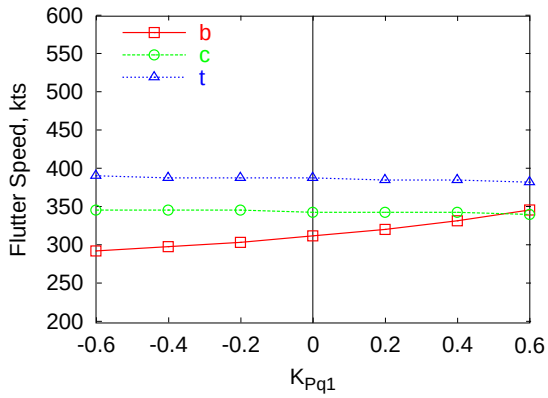

Figure 22: Influence of wing vertical bending-torsion coupling on flutter speed

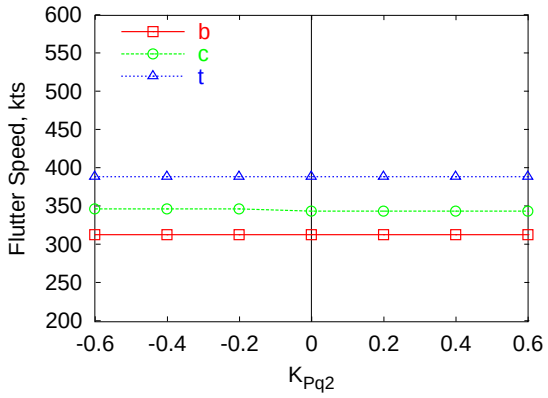

Figure 23: Influence of wing chordwise bending-torsion coupling on flutter speed

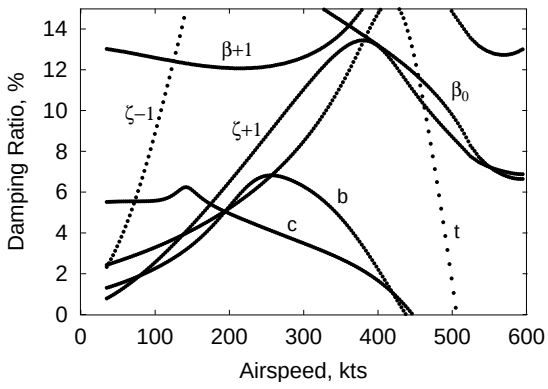

Figure 24: Rotor Optimization: Maximize damping from 200 to 600 kts (tight constraints)

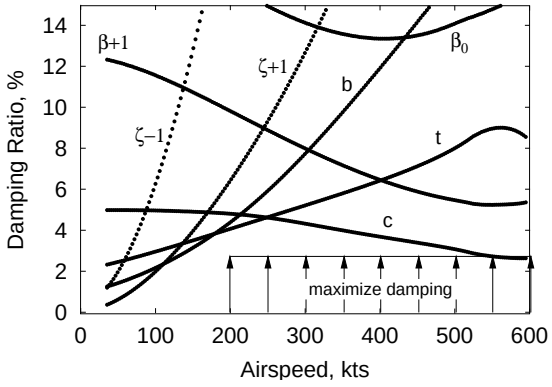

Figure 25: Rotor Optimization: Maximize damping from 200 to 600 kts (medium constraints)

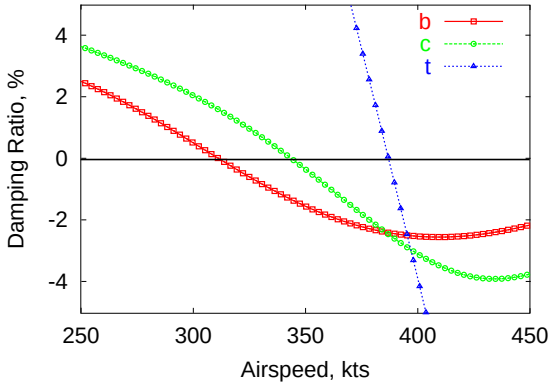

Figure 28: Wing design optimization: Optimization unable to improve beam mode damping, due to chord mode and torsion mode instabilities at high speeds

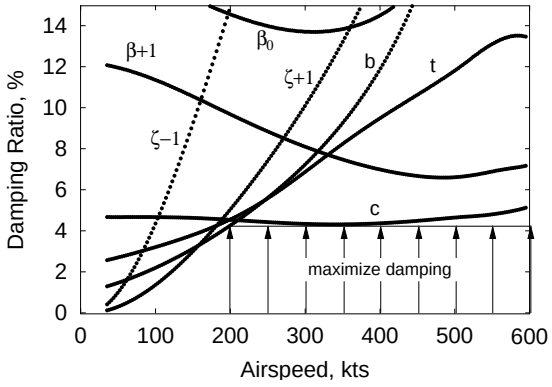

Figure 26: Rotor Optimization: Maximize damping from 200 to 600 kts (relaxed constraints)

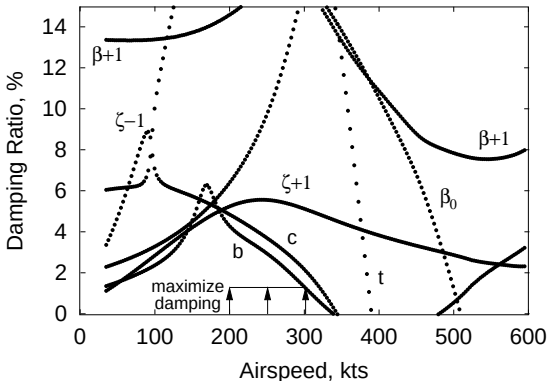

Figure 29: Wing Optimization: Maximize damping from 200 to 300 kts (tight constraints)

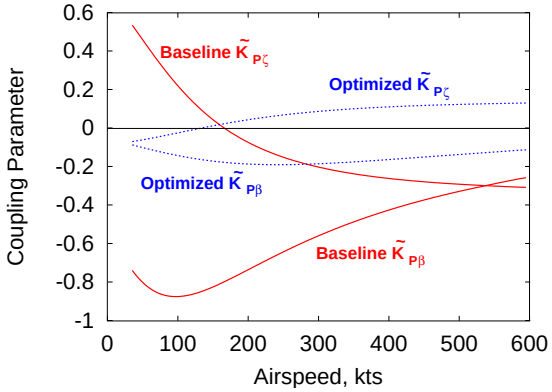

Figure 27: Rotor Optimization: Variation of pitch-flap and pitch-lag couplings due to distribution of blade flexibility

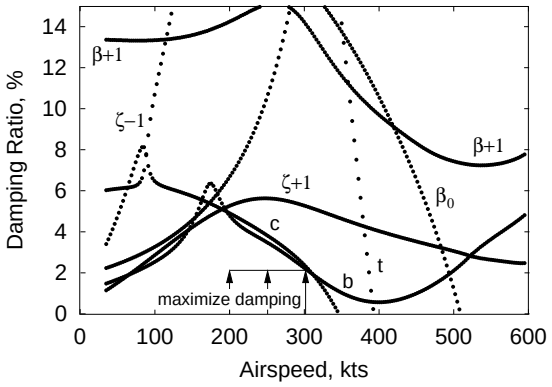

Figure 30: Wing Optimization: Maximize damping from 200 to 300 kts (medium constraints)

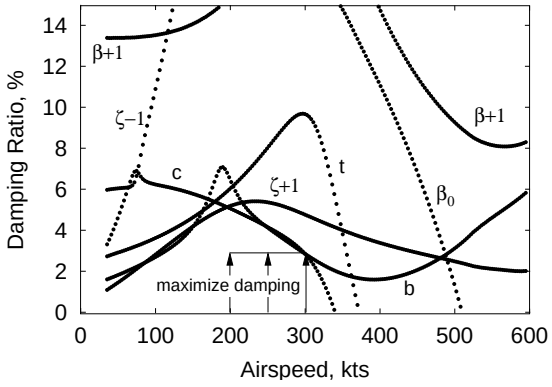

Figure 31: Wing Optimization: Maximize damping from 200 to 300 kts (relaxed constraints)

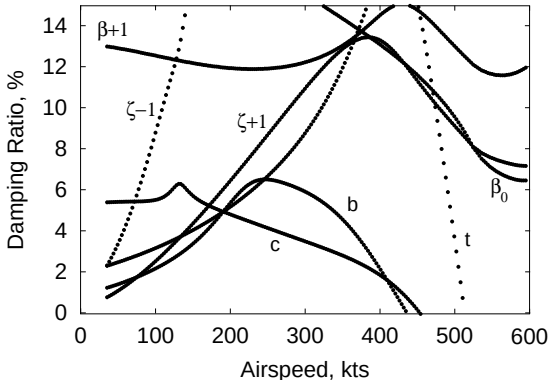

Figure 32: Concurrent Wing/Rotor Optimization: Maximize damping from 200 to 600 kts (tight constraints)

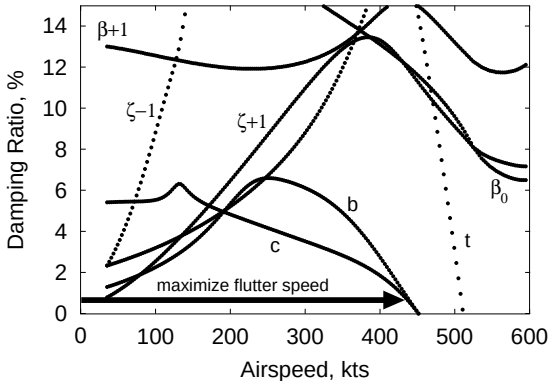

Figure 33: Concurrent Wing/Rotor Optimization: Maximize critical flutter speed (tight constraints)

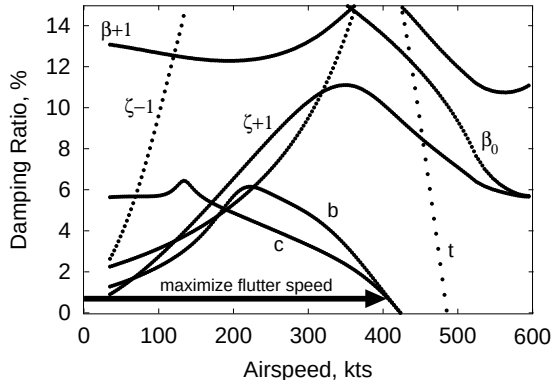

Figure 34: Concurrent Wing/Rotor Optimization: Maximize critical flutter speed (tight constraints, key parameters only)